



Degradation of *p*-nitrophenol (PNP) in aqueous solution by Fe⁰-PM-PS system through response surface methodology (RSM)

Jun Li, Qi Liu, Qing qing Ji, Bo Lai*

Department of Environmental Science and Engineering, School of Architecture and Environment, Sichuan University, Chengdu 610065, China



ARTICLE INFO

Article history:

Received 24 May 2016

Received in revised form 5 July 2016

Accepted 18 July 2016

Available online 19 July 2016

Keywords:

p-Nitrophenol (PNP)

Response surface methodology (RSM)

Synergistic effect

Degradation pathway

Reaction mechanism

ABSTRACT

To develop a technology for the degradation of the toxic and refractory pollutants, the Fe⁰-PM-PS system and 6 control experiments were setup in this study. First, effects of Fe⁰ dosage (0–18.3 g/L), PM dosage (0–25.0 mmol/L), PS dosage (0–30.0 mmol/L), initial pH value (3.0–11.0), air flow rate (0–2.0 L/min), and feeding times of PM and PS (1–5) on the degradation of PNP in aqueous solution by the Fe⁰-PM-PS system were studied through the single-factor experiment. Furthermore, the optimized experimental conditions (i.e., Fe⁰ dosage of 11.9 g/L, PM dosage of 15.0 mmol/L, PS dosage of 18.1 mmol/L and feeding times of oxidants of 4) were obtained through response surface methodology (RSM). The result shows that the maximum COD removal efficiency (89.0%) was obtained by the Fe⁰-PM-PS system under the optimal conditions, which was mainly attributed to the strong synergistic effect among Fe⁰, PM and PS. In addition, PNP degradation pathway was proposed according to the intermediates detected by HPLC. According to the analysis results of SEM-EDS, XRD and XPS, the reaction mechanism of the Fe⁰-PM-PS system has been clarified thoroughly. In short, these results suggest that the Fe⁰-PM-PS system should be proposed as an effective pretreatment process for the toxic and refractory PNP wastewater.

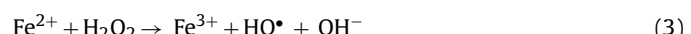
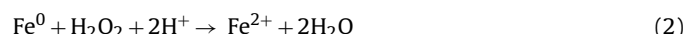
© 2016 Elsevier B.V. All rights reserved.

1. Introduction

For decades, since the toxic and intractable wastewater from industrial production is hard to be degraded completely, the intermediates and some unchanged forms of these compounds discharged into the ecosystem make a large challenge to the environment. In this study, *p*-nitrophenol (PNP), an important organic chemical raw material, was used as the model pollutant. It is the typical compound which is difficult to be degraded directly and its derivatives are the representative aromatic pollutants discharged from dyes, explosives, plasticizers and herbicides industries [1,2].

Over the last decades, application of zero valent iron (ZVI or Fe⁰, $E_0 = -0.44$ V) as an adsorbent and reducing agent in the treatment of contaminants has been extensively reported [3]. The removal of contaminants by ZVI is mainly attributed to the common effect of reduction, oxidation, adsorption, co-precipitation etc. [3–5]. On one hand, electron will transfer from ZVI to other contaminants which are changed into non-toxic or less toxic materials [6]. On the other hand, ZVI can degrade a series of organic compounds since

ZVI transfers two electrons to O₂ to produce H₂O₂ (Eq. (1)) [7]. The produced H₂O₂ can be reduced to water by another two-electron transfer from ZVI (Eq. (2)) [7]. Moreover, the combination of H₂O₂ and Fe²⁺ can produce hydroxyl radical (HO[•]) (Eq. (3)) [3,7]. However, the excess Fe²⁺ would scavenge HO[•] through Eq. (4). In the pH range pertaining to natural waters, Fe²⁺ may form Fe(OH)₂ and Fe(OH)₃ which could remove the pollutants through adsorption and co-precipitation [5].

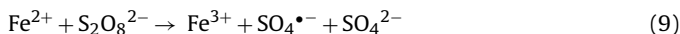
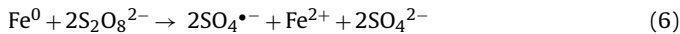
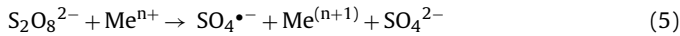


Advanced oxidation processes (AOPs), such as photocatalysis [8,9], ozonation [10,11], US/Fenton [12], and UV/Fenton [13], are regarded as the promising techniques for the degradation of recalcitrant organic pollutants based on the generation of HO[•] ($E_0 = 2.8$ V) and other free radicals. Recently, persulfate (PS, S₂O₈²⁻, $E_0 = 2.01$ V) which is a strong two-electron oxidizing agent has won the general attention. It has been reported that sulfate radical (SO₄^{•-}, $E_0 = 2.6$ V) is a stronger radical which can degrade most of the organic pollutants in water and exhibit stronger oxidative ability than HO[•].

* Corresponding author.

E-mail address: laibo@scu.edu.cn (B. Lai).

[14,15]. PS is used to generate $\text{SO}_4^{\bullet-}$ because of its high solubility in water, non-selective behavior and stability in environment conditions. Several PS activation methods have been studied, such as photolysis [15], microwaves [16], heat [17], electron beam [18,19], ultrasonication [20], alkaline [21], transition metal ions (Me^{n+}) [22,23] and zero-valent iron (ZVI) [24]. Particularly, PS chemical activation by transition metal irons is shown in Eq. (5). Similar to transition metal ions, ZVI can also activate PS to produce $\text{SO}_4^{\bullet-}$ at ambient temperature. In general, Fe^0 not only serves as a releasing source of dissolved Fe^{2+} , but also provides another way that involves direct electron transfer from ZVI to PS to produce $\text{SO}_4^{\bullet-}$. And the major reactions associated with ZVI and activation of PS are expressed as Eqs. (6)–(9) [25–27]. However, the excess Fe^{2+} presented in the activated system results in the scavenging of $\text{SO}_4^{\bullet-}$ through Eq. (10) [28].



Permanganate (PM) is a quite mild oxidizing agent with selective oxidizing capacity to some organic pollutants. Compared to other chemical oxidants, permanganate has some advantages such as the fact that it is easy to handle, safe storage and delivery [29]. Especially, potassium permanganate has been used to different fields since its discovery in 1659, such as catalysis, medicine and electrochemical and mechanical areas [30]. In addition, there have been reported that PM can oxidize some emerging environmental micro-pollutants, such as chlorophenol, bisphenol A and sulfamethoxazole [31]. Sun and his coworkers have found that PM can be activated by HSO_3^- , resulting in a process that oxidizes organic pollutants at extraordinarily high rate [32]. Besides, PM and its reduction products (e.g., Mn^{4+} , Mn^{3+} , Mn^{2+} , etc.) can be used to activate PS [33].

Response surface methodology (RSM) is an efficient and flexible experimental design technique for the modeling and analysis of problem in which a response of interest is influenced by several variables [34]. Compared to conventional optimization method, RSM is an economic and time-saving technology for it can provide more information from less number of experiments. RSM has been widely used to describe the interactive and synergistic effects among experimental variables as well as operation conditions optimization [35].

In this study, statistical experimental design and RSM were first applied to optimize the pertinent parameters related to COD removal efficiency of PNP in aqueous solution by Fe^0 -PM-PS system. We systematically evaluated the degradation of PNP in aqueous solution by RSM to get maximum COD removal efficiency. Meanwhile, effects of key factors including Fe^0 dosage, PM dosage, PS dosage, initial pH value, air flow rate and feeding times of PM and PS on the COD removal efficiency of PNP in aqueous solution were optimized in detail. The objectives of the study are to (1) provide an efficient technology for treatment of wastewater and determine the optimal parameters of Fe^0 -PM-PS process by RSM, (2) explore the synergistic functions of Fe^0 -PM-PS system, (3) illustrate the reasonable degradation mechanism with synergistic technology. The outcomes of this study may help to find new applications for the degradation of refractory wastewater.

2. Materials and methods

2.1. Reagent

p-Nitrophenol (PNP, 99%), zero valent iron (ZVI, Fe^0) powders, sodium persulfate (PS) from Chengdu Kelong chemical reagent factory, and potassium permanganate (PM) from Changjian chemical reagent factory were used in the experiment. The zero valent iron powders have a mean particle size of approximately 120 μm , and their iron content was above 98%. Other chemicals used in the experiment were of analytical grade. Deionized water was used throughout the whole experiment process. All solutions in the study were prepared by the deionized water.

2.2. Experimental procedure

PNP aqueous solution (500 mg/L) was prepared by simple dissolution in deionized water. In each experiment, 300 mL PNP aqueous solution was added in a 500 mL beaker. The pH of PNP aqueous solution was adjusted with 0.01 M H_2SO_4 /NaOH solution. The reaction was initiated as the simultaneous addition of ZVI powder, PM and PS. Besides, PM and PS were added to the solution at set intervals. During the reaction, the solution was stirred continuously and the whole experiment was performed at $25 \pm 2^\circ\text{C}$ by water bath heating. Besides, the samples were taken out at predetermined time intervals, and filtered through a 0.45 μm filter membrane. In particular, 100 μL methanol (1.0 mol/L) would be added into the samples before HPLC analysis of the filtrates [36]. The experiment included two steps: first single-factor experiment as the step I, second RSM design as step II. Firstly, in order to consider the impact of Fe^0 dosage, PM dosage, PS dosage, initial pH value, air flow rate and feeding times of PM and PS on treatment process, single-factor experiments were done, respectively. Secondly, on the basis of single-factor experiments, the CCD (Central Composite Design) experiment, one of the principal response surface methodologies used in experimental design, were done to obtain the optimal parameters.

2.3. Analytical methods

The surface morphologies of reacted ZVI in Fe^0 system, reacted ZVI particles and generated flocculation in Fe^0 -PM-PS system were observed by JSM-7500F field emission scanning electron microscopy (FE-SEM, JEOL Ltd., Japan). Besides, the surface elementary composition of ZVI particles and generated flocculation were analyzed by energy dispersive spectrometer (EDS). EDS analysis was carried out by a permanent thin film window link (Oxford Instrument) detector and WinEDS software in a JSM-7500F field emission scanning electron microscopy (FE-SEM). This instrument was operated at 25 kV and emission current of 60–70 μA subsequently. In addition, the flocculation by Fe^0 -PM-PS system was further investigated by X-ray diffraction (XRD) EMPYREAN diffractometer (PANalytical B.V., Holland). X-ray photoelectron spectroscopy (XPS, AXIS Ultra DLD, Kratos Co., UK) was used to identify the chemical states of Fe, Mn, O and S in the flocculation of Fe^0 -PM-PS system. The UV-vis absorption spectra of the effluent were carried out in 10 mm quartz cuvettes by UV-vis spectrophotometer (Shimazu, Japan), and the UV-vis spectra were recorded from 190 to 500 nm using deionized water as blank.

The concentration of PNP, *p*-aminophenol (PAP), Fumaric acid, Maleic acid, Hydroquinone (HC) and *p*-benzoquinone (BQ) in the samples was achieved by reversed-phase HPLC chromatography (Agilent USA) equipped with the Eclipse XDB C-18 (5 μm , 4.6 \times 250 mm). The binary phase were (A) water with 0.1% H_3PO_4 and (B) acetonitrile, and the eluent was A and B (1:1, v/v) with a flow rate of 1.2 mL/min. Detection was performed by a G1365MWD UV

detector set at 317 nm, 273 nm, 208 nm, 218 nm, 288 nm, 246 nm for PNP, PAP, Fumaric acid, Maleic acid, HC and BQ. The total Mn or Fe concentration of the treatment effluent was detected by an atomic absorption spectroscopy (AA-6300, Shimadzu, Japan). The treatment effluents of the experiments were analyzed by COD analyzer (Lianhua, China).

2.4. Experimental design

The response surface (RSM) is a statistical and mathematical method. In literature, the optimal parameters of the experiment for desirable can be determined and the interactions between significant parameters via two and three dimensional plots could be depicted [37]. Central composite design (CCD) is one of the excellent tools to establish RSM model.

To investigate the effects of pertinent operating parameters (Fe^0 dosage, PM dosage, PS dosage and feeding times of PM and PS) on the COD removal efficiency, the CCD design was applied to determine the optimal levels of the significant factors and the interactions of such variables. A four factor, five-level CCD with 30 runs was employed, and the five coded levels of each variable were designated as $-\alpha$, -1 , 0 , $+1$, $+\alpha$. The experiments were performed in a random manner in order to reduce any systematic bias due to extraneous factors.

Analysis of variance (ANOVA) was applied for statistical analysis of experimental data for the determination of the model [38,39]. The coefficients of the model, which were calculated by a multiple regression analysis on the experimental data, were analyzed to evaluate if the given term has a significant effect ($p \leq 0.05$). In this paper, Design-Expert version 8.05b was used to design experiments and to analyze the regression and graphical experimental data obtained.

3. Results and discussion

3.1. Parameters optimization (single factor experiments)

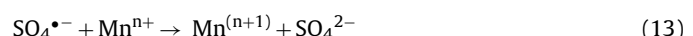
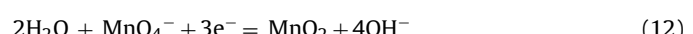
3.1.1. Effects of Fe^0 dosage

Effects of Fe^0 dosage (0, 5.0, 10.0, 12.0, 13.3, 15.0, 16.7, 18.3 g/L) on the COD removal efficiency of PNP aqueous solution were evaluated. Fig. 1(a) indicates that the COD removal efficiency increased from 19.6% to 79.3% after 120 min treatment when the Fe^0 dosage increased from 0 to 13.3 g/L. The above results can be explained from the following aspects: (i) The total surface area of Fe^0 increase with increasing Fe^0 dosage, which make a contribution to enhance the corrosion and adsorption of iron. (ii) Corrosion products (e.g., Fe^{2+} , Fe^{3+} , $FeOOH$, Fe_3O_4 , etc.) was increasing in acid condition with the increasing of Fe^0 dosage, and they can activate PS to generate sulfate radical that can degrade the pollutants [33,40]. (iii) Essential Fe^0 was needed to efficiently form the Fenton-like reaction in the present of dissolved oxygen (DO) (Eqs. (1)–(3)) [7]. Oxygen would be dissolved into reaction solution due to the mechanical agitation when the experiment process was explored in air [13]. However, the treatment efficiency decreased from 79.3% to 16.4% when Fe^0 dosage further increased from 13.3 g/L to 18.8 g/L. The results suggest that if the catalyst (i.e., Fe^0 and its corrosion products) exceeds the optimum, then the generated radicals are scavenged from Eqs. (4) and (10) and the degradation rate declines consequently [41–43]. Therefore, the optimal Fe^0 dosage of 13.3 g/L was selected in the sequential experiments to investigate the effect of PM on the COD removal.

3.1.2. Effects of PM dosage

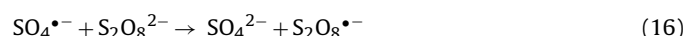
Effects of PM dosage (0, 5.0, 10.0, 15.0, 20.0, 22.5, 25.0 mmol/L) on the COD removal efficiency of PNP aqueous solution were evaluated. Fig. 1(b) shows that an increase of PM dosage from 0 to

10.0 mmol/L improved the COD removal efficiency, and it reached the maximum at the PM dosage of 10.0 mmol/L. The results can be illustrated from three aspects: (i) PNP and its intermediate can be directly oxidized by PM [32]. (ii) The increasing of PM ($Mn(VII)$) dosage would produce more low valance state Mn^{n+} ions or manganese oxides due to the reduction of PM (e.g., Eqs. (11) and (12)), which can activate PS and H_2O_2 to generate the radicals (e.g., HO^\bullet and SO_4^{2-}) that can rapidly degrade PNP [33,44–48]. (iii) Meanwhile, the in situ Mn -Fe oxide ($MnFe_2O_4$) by dissolved $Mn(II)$ complexing or co-precipitating with iron oxide promoted the adsorption of pollutants [49]. However, a further increase of PM dosage to 20.0 mmol/L did not increase the COD removal efficiency, which reduced to 31.4% when PM dosage reached 25.0 mmol/L. This could be ascribed to the competitive consumption of the generated radicals (e.g., HO^\bullet and SO_4^{2-}) with excess dissolved Mn^{n+} ions generated according to Eqs. (13) and (14) [27]. Therefore, the optimal PM dosage was chose as 10.0 mmol/L.



3.1.3. Effects of PS dosage

Effects of PS dosage (0, 5.0, 10.0, 15.0, 20.0, 25.0, 30.0 mmol/L) on COD removal efficiency of PNP aqueous solution were evaluated. It could be seen from Fig. 1(c) that the COD removal efficiency increased and peaked at 84.7% when the PS dosage was increased to 20.0 mmol/L, while PS exceeding the dosage of 20.0 mmol/L reduced the COD removal efficiency of the Fe^0 -PM-PS system due to the consumption of SO_4^{2-} by excess PS or SO_4^{2-} (Eqs. (15) and (16)) [22,50,51]. Meanwhile, the similar phenomena have been found in the ZVI-PS, Fe^{2+} -PS systems [50,52]. In addition, the excess PS would rapidly decrease the solution pH because plenty of H^+ was released from the decomposition of PS (Eqs. (17)–(19)) [51]. The plenty of H^+ would enhance seriously the corrosion of Fe^0 and release excess Fe^{2+} . Subsequently, the excess Fe^{2+} would scavenge the generated radicals (Eqs. (4) and (10)). Finally, the optimal PS dosage was selected as 20.0 mmol/L.



3.1.4. Effects of pH value

Fig. 1(d) shows the effect of initial pH on COD removal efficiency by the Fe^0 -PM-PS system. This system effectively decompose the PNP aqueous solution at a broad pH range of 3.0–11.0, at which more than 80.0% of COD removal efficiency was obtained within 120 min. The COD removal under various pH did not significantly differ, the acidic pH was more favorable than alkaline and neutral conditions. For example, COD removal (85.7%) obtained at an initial pH of 5.0 was higher than that (79.9%) obtained at an initial pH of 11.0.

In literature, it is reported that the generated SO_4^{2-} would further undergo reactions with OH^- or H_2O to form HO^\bullet under alkaline, neutral or acidic conditions (Eqs. (19) and (20)) [51]. Studies have reported that sulfate radical predominated under acidic conditions while the hydroxyl radical was more prominent under basic conditions [53]. Furthermore, the acidic initial pH could favor the corrosion of Fe^0 and release more Fe^{2+} that could activate the PS, while alkaline pH would inhibit the release of Fe^{2+} . In particular,

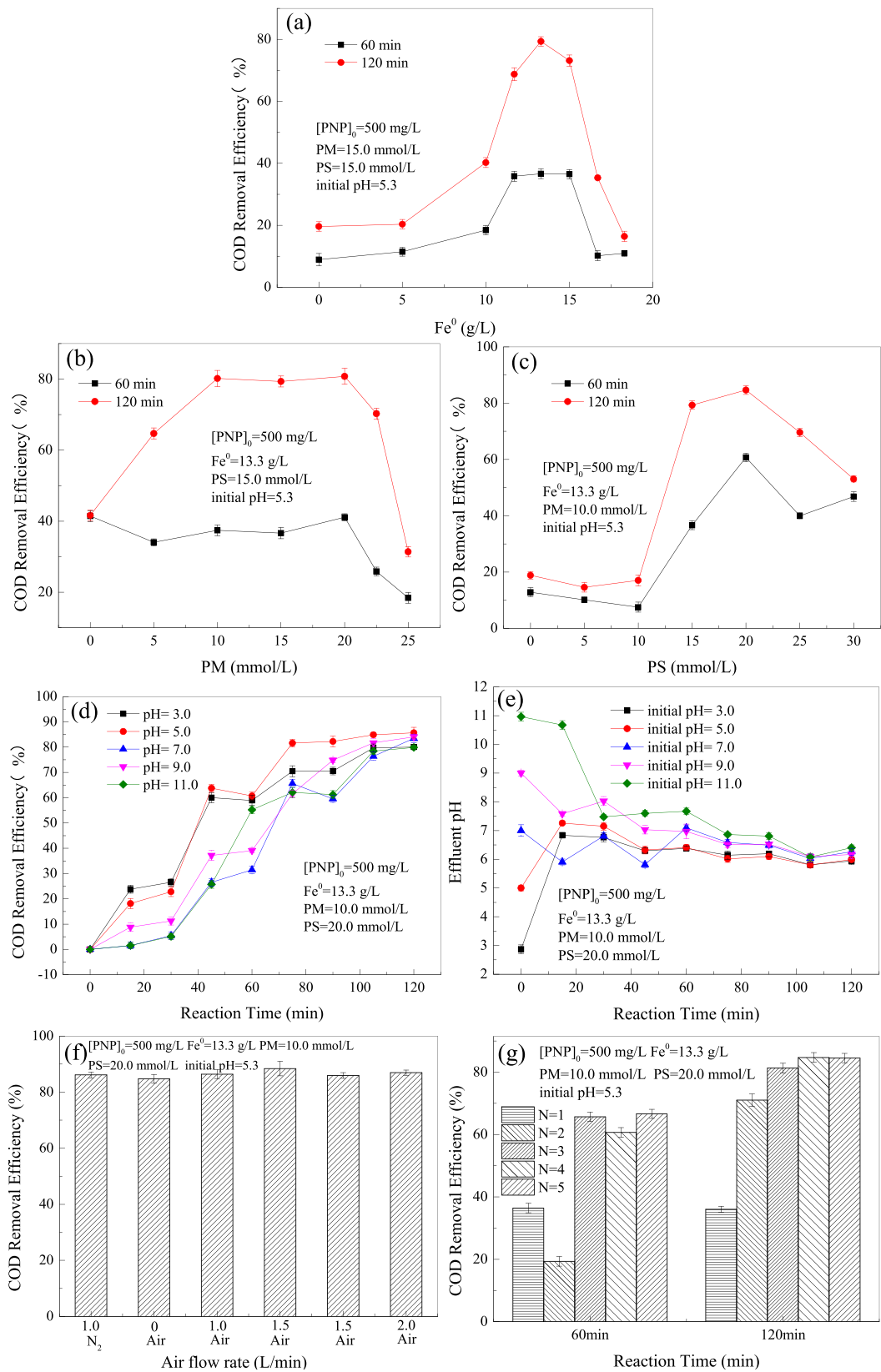


Fig. 1. Effects of (a) Fe⁰ dosage, (b) PM dosage, (c) PS dosage, (d) initial pH value, (f) air flow rate and (g) feeding times of PM and PS on the COD removal of PNP aqueous solution. (e) Variation of solution pH during the treatment process with different initial pH.

when the initial pH of 5.0 was the most close to the pH of 500 mg/L PNP aqueous solution (i.e., pH=5.3), the COD removal efficiency reached to 85.7%. Therefore, the optimal initial pH was the pH of 500 mg/L PNP aqueous solution (i.e., pH=5.3) for the Fe⁰-PM-PS system.

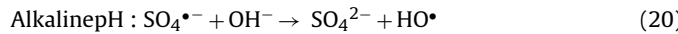


Fig. 1(e) shows variation of solution pH during the 120 min treatment process with different initial pH values (3.0, 5.0, 7.0, 9.0, 11.0). It is clear that the effluent pH of all batch experiments with different initial pH was around 6.0 after 120 min treatment process. Under the acidic conditions (the initial pH < 6.0), H⁺ could be consumed through the corrosion reaction of Fe⁰, leading to the increase of effluent pH. However, under the alkaline conditions (the initial pH > 7.0), the OH⁻ would be consumed according to Eqs. (19) and (20). Furthermore, some carboxyl acids intermediates might be generated in the treatment process by Fe⁰-PM-PS system, which made the solution pH decrease. Zou and his colleagues also found the similar results that a final solution pH of 6.5 in the US/Fe⁰/PS system was measured [51].

3.1.5. Effects of air flow rate

It is reported that Fenton-like reaction usually occurs in the Fe⁰/air system, and facilitates the degradation of the pollutants [7]. Thus, the effects of air flow rate (0, 0.5, 1.0, 1.5, 2.0 L/min) on the COD removal efficiency of PNP aqueous solution by Fe⁰-PM-PS system were evaluated thoroughly. Meanwhile, a control experiment with a nitrogen flow rate of 1.0 L/min was set up to further confirm the performance of the dissolved oxygen (DO). **Fig. 1(f)** shows that the COD removal efficiency remained between 85.1% and 88.4% under different aeration conditions (i.e., N₂, air or without aeration). The results suggest that effect of DO on the COD removal efficiency by Fe⁰-PM-PS system could be neglected completely. In other words, the Fenton-like reaction from Fe⁰ in present of DO did not contribute to the COD removal efficiency in the Fe⁰-PM-PS system. Therefore, Fe⁰-PM-PS system was carried out without aeration.

3.1.6. Effects of feeding times of PM and PS

Effects of feeding times of PM and PS (N=1–5) on the COD removal efficiency of PNP aqueous solution was evaluated. As shown in **Fig. 1(g)**, after 120 min treatment by Fe⁰-PM-PS system, up to 36.0%, 71.0%, 81.3%, 84.7%, 84.5% of COD removal efficiency had attained with the sequential feeding times of PM and PS for N=1–5, respectively. The results illustrate that COD removal efficiency was remarkably improved through the portion-wise addition of PM and PS (N≥3) during the 120 min treatment process. The results could be explained from three aspects, (i) The one-time addition of all PM and PS would cause the excess oxidants including their activated products (e.g., SO₄^{•-}) in the reaction solution. They are hard to be completely used to decompose the pollutants in aqueous solution, and the excess oxidants would be scavenged by themselves and Fe⁰ (Eqs. (4) and (8)) [27,28,54]. (ii) The excess PS would release the excess H⁺ that would rapidly accelerate the corrosion rate of Fe⁰ and generate excess Fe²⁺/Fe³⁺ ions, which could be used as scavengers for SO₄^{•-} and HO[•] [33]. (iii) The excess PM would be rapidly consumed by Fe⁰ or Fe²⁺ to generate Mnⁿ⁺ (e.g., 2+, 3+, 4+, etc.) ions (Eqs. (11) and (12)) [32], which would be used as scavengers for SO₄^{•-} and HO[•] (Eqs. (13) and (14)) [27,33]. Therefore, the optimal feeding times of PM and PS was determined as 4 (i.e., adding PM and PS at 30 min interval in the whole 120 min treatment process).

3.2. Parameters optimization (response surface methodology (RSM))

On the basis of the above optimal parameters (i.e., Fe⁰ dosage of 13.3 g/L, PM dosage of 10.0 mmol/L, PS dosage of 20.0 mmol/L, initial pH of 5.3, feeding times of PM and PS was 4) obtained from the single-factor experiments, the interaction among the four key parameters (Fe⁰ dosage, PM dosage, PS dosage and feeding times) were investigated thoroughly by RSM. The results obtained from the run of 30 experimental sets, suggested by CCD models of RSM, were analyzed by software. Subsequently, analysis of variance (ANOVA), regression coefficients and polynomial regression equation were obtained. Results of the experimental matrix of corresponding CCD design are presented in **Table 1**. Consequently, all linear terms of A (Fe⁰ dosage), B (PM dosage), C (PS dosage), D (feeding times), and the quadratic terms of A², B², C², D² and interaction terms of AB, AC, AD, BC, BD, CD were considered as relevant parameters of COD removal efficiency of PNP aqueous solution by Fe⁰-PM-PS system.

As presented in **Table 2**, the “Model F-value” of 11.15 and the value of “Prob>F” for the quadratic model indicated that the model was significant and there was only 0.01% chance that the “Model F-value” could have been occurred as the result of noise. The value of “Prob>F” for the model, being less than 0.05 (<0.0001), implied that the model was statistically significant. The lack of fit of the model indicates if the calculated response surface represents the true shape of the surface [55]. It should be noted that the “Lack of Fit p-value” was 0.1829, suggesting that the lack of fit was not significant and the model had a good predictability. Besides, the value of R² and “Adeq Precision” reached 0.9123 and 13.655, respectively. It indicated that the model had a good degree of fitting and the signal to noise ratio was adequate (>4). Thus, the model may be summarized as a simultaneous function of Fe⁰ dosage (A), PM dosage (B), PS dosage (C) and feeding times of PM and PS (D) as follows:

$$\begin{aligned} \text{CODremovalefficiency}(\%) = & +60.46 + 6.73 \times A + 0.87 \times B \\ & + 12.78C + 4.95D + 2.93 \times A \times B - 2.14 \times A \times C + 1.68 \times A \times D \\ & + 4.51 \times B \times C - 0.22 \times B \times D \\ & + 2.40 \times C \times D - 3.20 \times A^2 - 0.38 \times B^2 - 3.11 \times C^2 - 2.00 \times D^2 \end{aligned}$$

All terms in the regression model are not equally important. Values of P less than 0.05 indicate model terms are significant. Values greater than 0.10 indicate the model terms are not significant [38]. The result of **Table 2** implies that the liner effects of A, C, D, interactive effects of AB, BC, and square effects of A², C² are important. After eliminating those insignificant terms from the regression equation and refining the model, the above empirical model equation may be simplified in terms of coded factors to:

$$\begin{aligned} \text{CODremovalefficiency}(\%) = & +60.46 + 6.73 \times A + 12.78C \\ & + 4.95D + 2.93 \times A \times B - 4.51 \times B \times C - 3.20 \times A^2 - 3.11 \times C^2 \end{aligned}$$

The predicted values of the model response versus actual values are shown in **Fig. 2**. The data points are distributed relatively close and have linear behavior, and the distance between the cluster points and diagonal line is regarded as small values. In addition, the higher R² value (0.99274) indicates a wonderful relationship between the actual and the predicted values of the response in COD removal efficiency obtained by Fe⁰-PM-PS system. The results further proved that the RSM model excellently fit with the experimental results.

According to the obtained RSM model, optimization of the four experimental parameters could be conducted. An optimal condi-

Table 1CCD design and response of COD removal efficiency of PNP aqueous solution by Fe^0 -PM-PS system.

Factors	levels and ranges				
	$-\alpha$	Low (-1)	Middle (0)	High (+1)	$+\alpha$
A: Fe^0 dosage (g/L)	2.5	5.0	7.5	10.0	12.5
B: PM dosage (mmol/L)	3.0	6.0	9.0	12.0	15.0
C: PS dosage (mmol/L)	4.0	8.0	12.0	16.0	20.0
D: Feeding times	1	2	3	4	5
Std	Run	A: Fe^0 dosage	B: PM dosage	C: PS dosage	D: Feeding times
1	3	5.0	6.0	8.0	2
2	17	10.0	6.0	8.0	2
3	5	5.0	12.0	8.0	2
4	13	10.0	12.0	8.0	2
5	8	5.0	6.0	16.0	2
6	1	10.0	6.0	16.0	2
7	21	5.0	12.0	16.0	2
8	22	10.0	12.0	16.0	2
9	20	5.0	6.0	8.0	4
10	6	10.0	6.0	8.0	4
11	28	5.0	12.0	8.0	4
12	7	10.0	12.0	8.0	4
13	24	5.0	6.0	16.0	4
14	30	10.0	6.0	16.0	4
15	15	5.0	12.0	16.0	4
16	4	10.0	12.0	16.0	4
17	19	2.5	9.0	12.0	3
18	29	12.5	9.0	12.0	3
19	12	7.5	3.0	12.0	3
20	10	7.5	15.0	12.0	3
21	14	7.5	9.0	4.0	3
22	25	7.5	9.0	20.0	3
23	18	7.5	9.0	12.0	1
24	26	7.5	9.0	12.0	5
25	23	7.5	9.0	12.0	3
26	16	7.5	9.0	12.0	3
27	27	7.5	9.0	12.0	3
28	9	7.5	9.0	12.0	3
29	2	7.5	9.0	12.0	3
30	11	7.5	9.0	12.0	3

Table 2

ANVOA (analysis of variance) for the optimized RSM model.

Source	Sum of Squares	df	Mean Square	F Value	p-value	prob > F
Model	6816.51	14	486.89	11.15	<0.0001	significant
A- Fe^0 dosage	1087.03	1	1087.03	24.89	0.0002	
B-PM dosage	18.17	1	18.17	0.42	0.5287	
C-PS dosage	3920.90	1	3920.90	89.78	<0.0001	
D-Feeding times	587.47	1	587.47	13.45	0.0023	
AB	137.48	1	137.48	3.15	0.0963	
AC	73.19	1	73.19	1.68	0.2151	
AD	45.29	1	45.29	1.04	0.3247	
BC	325.98	1	325.98	7.46	0.0154	
BD	0.79	1	0.79	0.018	0.8947	
CD	92.35	1	92.35	2.11	0.1665	
A^2	281.05	1	281.05	6.44	0.0228	
B^2	3.93	1	3.93	0.090	0.7683	
C^2	265.04	1	265.04	6.07	0.0263	
D^2	109.28	1	109.28	2.50	0.1345	
Residual	655.11	15	43.67			
Lack of Fit	538.92	10	53.89	2.32	0.1829	not significant
Pure Error	116.19	5	23.24			
Cor Total	7471.62	29				
Std.Dev.	6.61		R^2		0.9123	
Mean	53.51		R_{Adj}^2		0.8305	
C.V.%	12.35		R_{Pred}^2		0.5621	
PRESS	3271.50		Adeq Precision		13.655	

tion of 11.9 g/L Fe^0 , 15.0 mmol/L PM, 18.1 mmol/L PS and feeding times of PM and PS of 4 was predicted. Validation experiments were performed in order to examine the validity of the statistical model and the optimal conditions. And the actual COD removal efficiency of 89.0% was achieved under the same optimized conditions.

Therefore, a good agreement between the model prediction and the experimental data may demonstrate the validity of the model, which manifests that the model is insensitive to external noise and valid to predict the experiment.

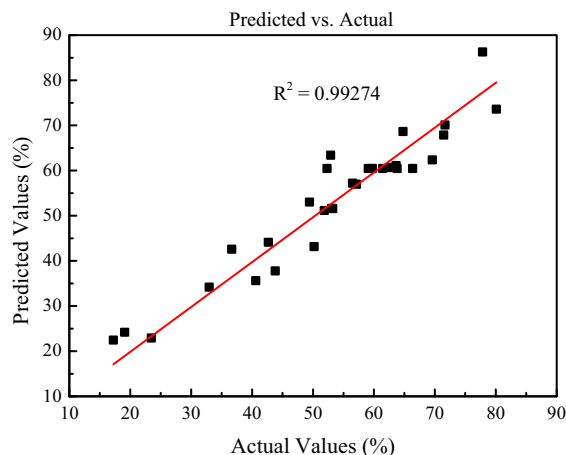


Fig. 2. The actual values plotted against the predicted values derived from the model of COD removal efficiency (%) from the experimental design.

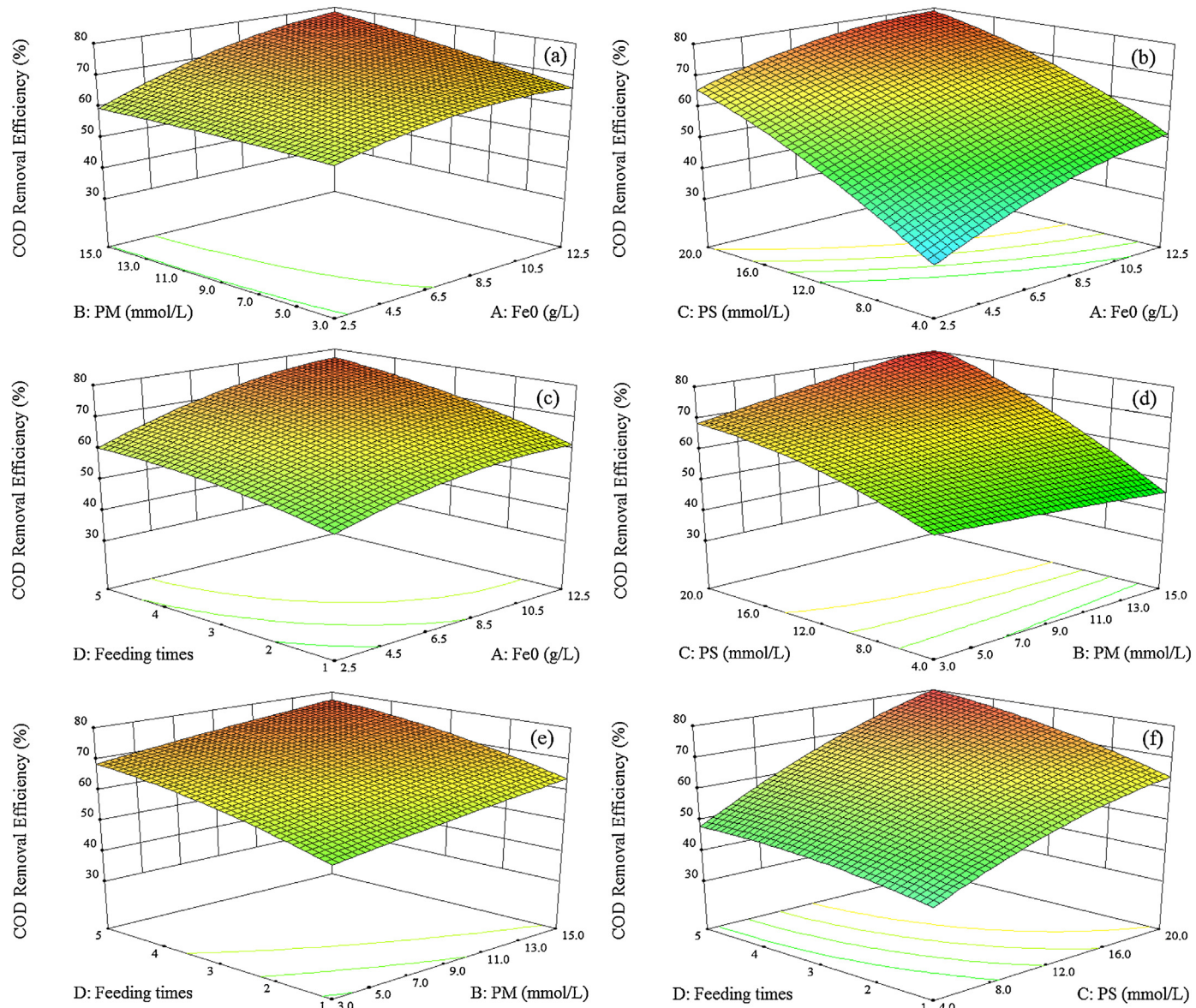


Fig. 3. Interactive relationships between (a) Fe^0 and PM, (b) Fe^0 and PS, (c) Fe^0 and Feeding times, (d) PM and PS, (e) PM and Feeding times, and (f) PS and Feeding times with the 3D response surfaces for the COD removal efficiency of PNP aqueous solution (500 mg/L) in the Fe^0 -PM-PS system.

3.3. Interactive relationship of Fe^0 , PM and PS

As the model established and optimized, the interactive relationships between Fe^0 and PM, Fe^0 and PS, PM and PS, Fe^0 and Feeding times, PM and Feeding times, PS and Feeding times were described. **Fig. 3** shows the 3D surface plots of the RSM study, which disclose the mutual interaction between parameters and response [56]. **Fig. 3(a)** illustrates the interactive relationship between Fe^0 and PM. It is evident that increasing the dosage of two chemicals in proportion would lead to gradual increase in the COD removal efficiency. Wang and his colleagues also found that the strong synergistic effect between ZVI and PM could enhance dye synergistic degradation [49]. **Fig. 3(b)** describes the interactive relationship between Fe^0 and PS. It can be seen that COD removal efficiency would increase with the augment of Fe^0 and PS dosage appropriately. Plenty of H^+ ions generated from the activation of PS (Eq. (18)) would facilitate the iron corrosion, and the generated corrosion products would accelerate the activation of PS in return [33,51]. However, Fe^0 dosage exhibited relatively lower impacts

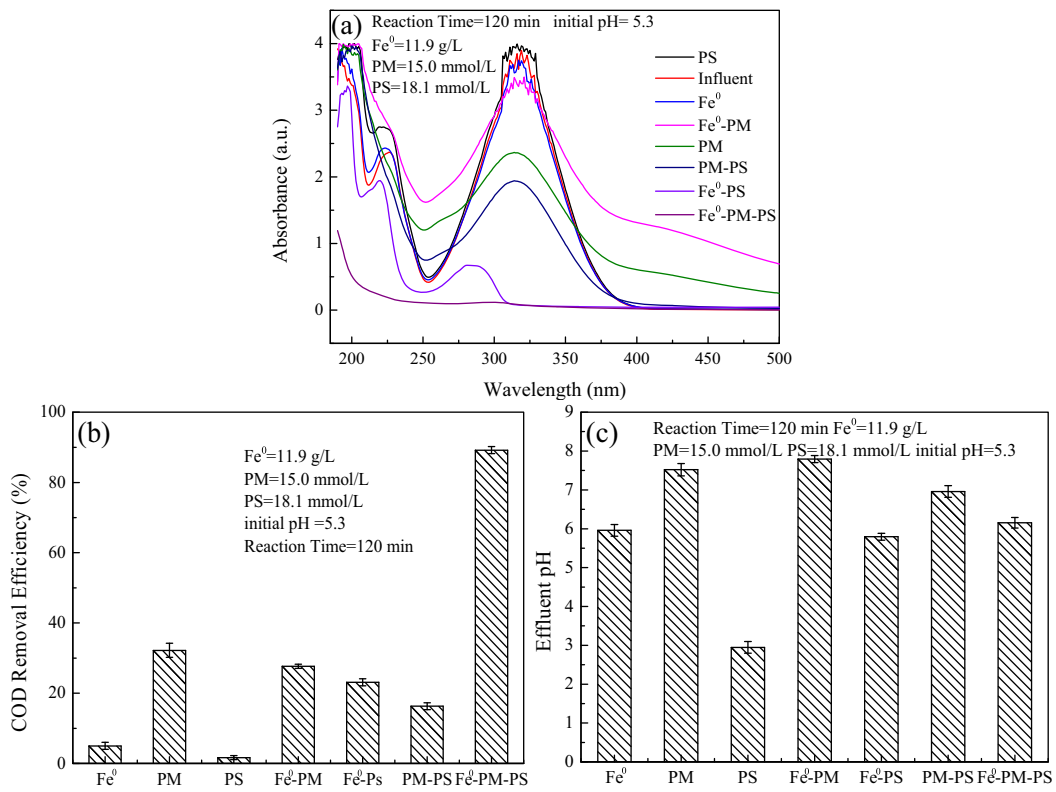


Fig. 4. UV spectra, COD removal and pH of the effluent of 7 different treatment processes.

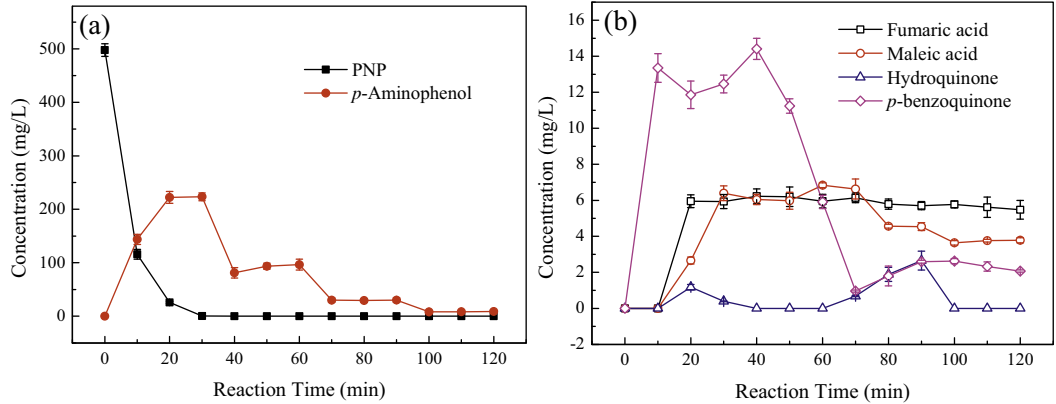


Fig. 5. PNP and its degradation intermediates measured in Fe⁰-PM-PS system.

at higher concentration levels compared to PS dosage, because the excess Fe⁰ and its corrosion would be used as scavengers for SO₄^{•-} and HO[•] (Eqs. (4) and (10)) [41–43]. Fig. 3(c) shows the interactive relationship between Fe⁰ and feeding times. The increasing of Fe⁰ dosage and feeding times would make a contribution to the improving of COD removal. The reason can be explained that the addition of PM and PS with equal time intervals into the reaction solution would make SO₄^{•-} produced persistently. Fig. 3(d) also shows the interactive relationship between PM and PS. Reduction products (e.g., Mnⁿ⁺ ions and MnO₂) of PM could activate PS effectively [33,45–48]. The similar results were reported that there was strong synergistic effect between PM and peroxymonosulfate (PMS) [44]. It can be seen from Fig. 3(e) and (f) that COD removal efficiency exhibit a continuous growth as the number of PM and PS portions added increased. The similar phenomenon has been reported in the literature [50]. That can be explained that the SO₄^{•-} could be produced abidingly in the whole treatment process compared to the

one-time addition of all PM and PS. The above discussion confirms the high treatment efficiency of Fe⁰-PM-PS system.

3.4. Superiority and synergistic effect of the Fe⁰-PM-PS process

To evaluate the superiority and synergistic effect of the Fe⁰-PM-PS process, six control experiments including (a) Fe⁰, (b) PM, (c) PS (d) Fe⁰-PM (e) Fe⁰-PS (f) PM-PS were set up under the same conditions (i.e., Fe⁰ dosage of 11.9 g/L, PM dosage of 15.0 mmol/L, PS dosage of 18.1 mmol/L, stirring speed of 250 r/min and reaction time of 120 min, reaction temperature of 25 °C, initial pH of 5.3).

The changes in UV absorbance characteristics of the influent and effluent of Fe⁰, PS, PM, Fe⁰-PS, Fe⁰-PM, PM-PS and Fe⁰-PM-PS systems from 190 to 500 nm were shown in Fig. 4(a). The peak at 227 nm is mainly attributed to the π–π* transition of benzene ring of monoaromatics, and the peak at 317 nm is mainly due to the conjugation of benzene ring and chromophoric group (i.e., –NO₂)

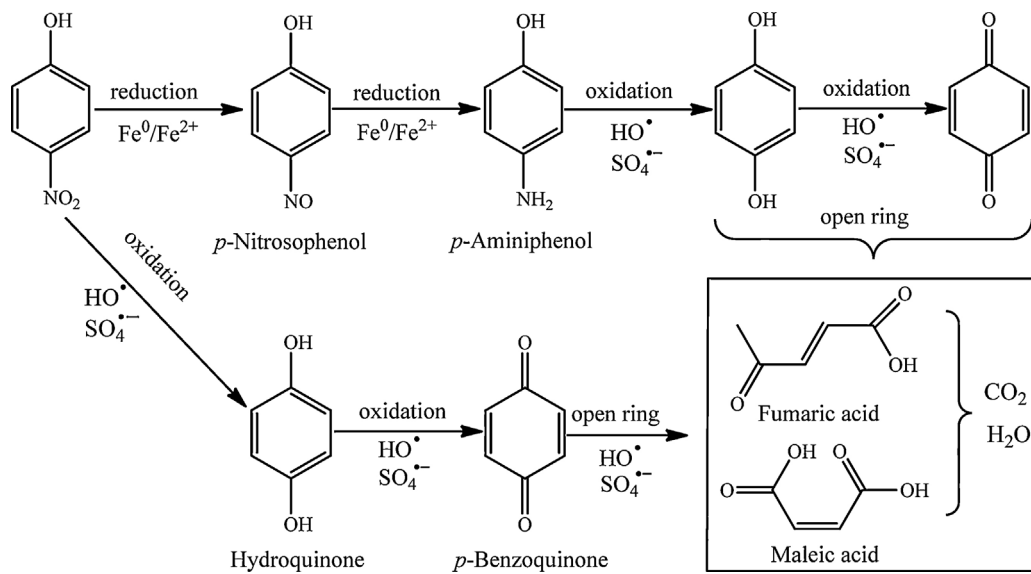


Fig. 6. Proposed reaction pathway for the degradation of PNP by the Fe^0 -PM-PS system.

[57]. Fig. 4(a) shows that the absorbance intensity of the peak at 227 nm and 317 nm of PNP aqueous solution dropped slowly in the Fe^0 , PS, PM, Fe^0 -PM, or PM-PS system, while all peaks were dropped remarkably in the Fe^0 -PM-PS system. The results reveal that only a little part of PNP can be removed by these systems (i.e., Fe^0 , PS, PM, Fe^0 -PM, or PM-PS), while both the benzene ring and nitro group of PNP could be decomposed effectively by the Fe^0 -PM-PS system. In addition, only the peak at 317 nm was dropped remarkably in the Fe^0 -PS system due to the rapid reduction of PNP and generation of *p*-aminophenol under acidic condition (H^+ ions was produced from the decomposition of PS) [6]. Thus the synergistic effect of the Fe^0 -PM-PS process played a leading role in the degradation of PNP in aqueous solution.

As shown in Fig. 4(b), the COD removal efficiencies of 5.0%, 32.2%, 1.7%, 27.7%, 23.1%, 16.3% and 89.0% were obtained by Fe^0 , PM, PS, Fe^0 -PM, Fe^0 -PS, PM-PS, and Fe^0 -PM-PS systems, respectively. In addition, COD removal efficiency obtained by the Fe^0 -PM-PS process (89.0%) was twice more than the sum (38.9%) of Fe^0 , PM and PS, and it was even much higher than the sum (67.1%) of Fe^0 -PM, Fe^0 -PS, PM-PS. The results also confirm that there is extremely strong synergistic effect in the Fe^0 -PM-PS system that was superior to other 6 treatment processes.

The effluent pH values of 7 different treatment processes were illustrated in Fig. 4(c). The effluent pH of PS system was decreased to 2.9, while all the effluent pH of other 6 systems was closed to neutral condition. These phenomena could be attributed to the following aspects: (i) The decomposition of PS would release plenty of H^+ ions to decrease the pH [40]. (ii) The generated H^+ ions could enhance the Fe^0 corrosion and generate plenty of $\text{Fe}^{2+}/\text{Fe}^{3+}$, which could increase the pH of reaction solution. In other words, the released H^+ ions could be utilized by Fe^0 effectively, which facilitate to improve the performance of the Fe^0 -PM-PS process.

3.5. Proposed reaction pathway for the destruction of PNP in Fe^0 -PM-PS system

In literatures, there are some reports on the degradation mechanism of PNP by AOPs [1,37,58]. The previous studies show that the benzene ring structure of *p*-benzoquinone would be opened by oxidation process and generated the small molecular organics (e.g., fumaric acid, maleic acid, acrylic acid etc.) that would be further degraded into CO_2 and H_2O [59]. The degradation interme-

diates detected in this study were *p*-aminophenol, hydroquinone, *p*-benzoquinone, and fumaric, and maleic acids. The concentration variation of each intermediate and the residual PNP during the 120 min treatment process by Fe^0 -PM-PS system are presented in Fig. 5. Fig. 5(a) shows that PNP had been removed completely in the initial 30 min treatment process, meanwhile the reduction product (i.e., *p*-aminophenol) was rapidly increased to the maximum (223 mg/L) at 30 min, and then it began to decrease gradually in the following 90 min treatment process. In addition, the concentration of *p*-benzoquinone also increased rapidly to the maximum (14 mg/L) at 40 min, and then it was further removed in following 80 min treatment process (Fig. 5(b)). Furthermore, Fig. 5(b) also shows that a little of fumaric acid, maleic acid and hydroquinone (<8 mg/L) were measured during the whole treatment process, which suggest that these intermediates could not be accumulated but could further decomposed rapidly.

According to the measured intermediates, the main degradation pathway is proposed in Fig. 6. In particular, two degradation pathways were proposed as following: (i) **combined reduction and oxidation**: PNP is first reduced to *p*-nitrosophenol by direct reduction of Fe^0 or Fe^{2+} , which is further reduced to *p*-aminophenol. Then *p*-aminophenol is oxidized to hydroquinone and *p*-benzoquinone by SO_4^{2-} and HO^\bullet . Moreover, their benzene rings are opened and further oxidized to ring opening compounds (e.g., fumaric acid and

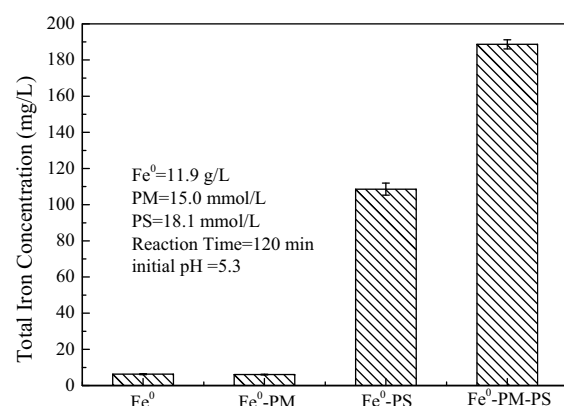


Fig. 7. Total iron ions concentration of the effluent in Fe^0 , Fe^0 -PM, Fe^0 -PS and Fe^0 -PM-PS system.

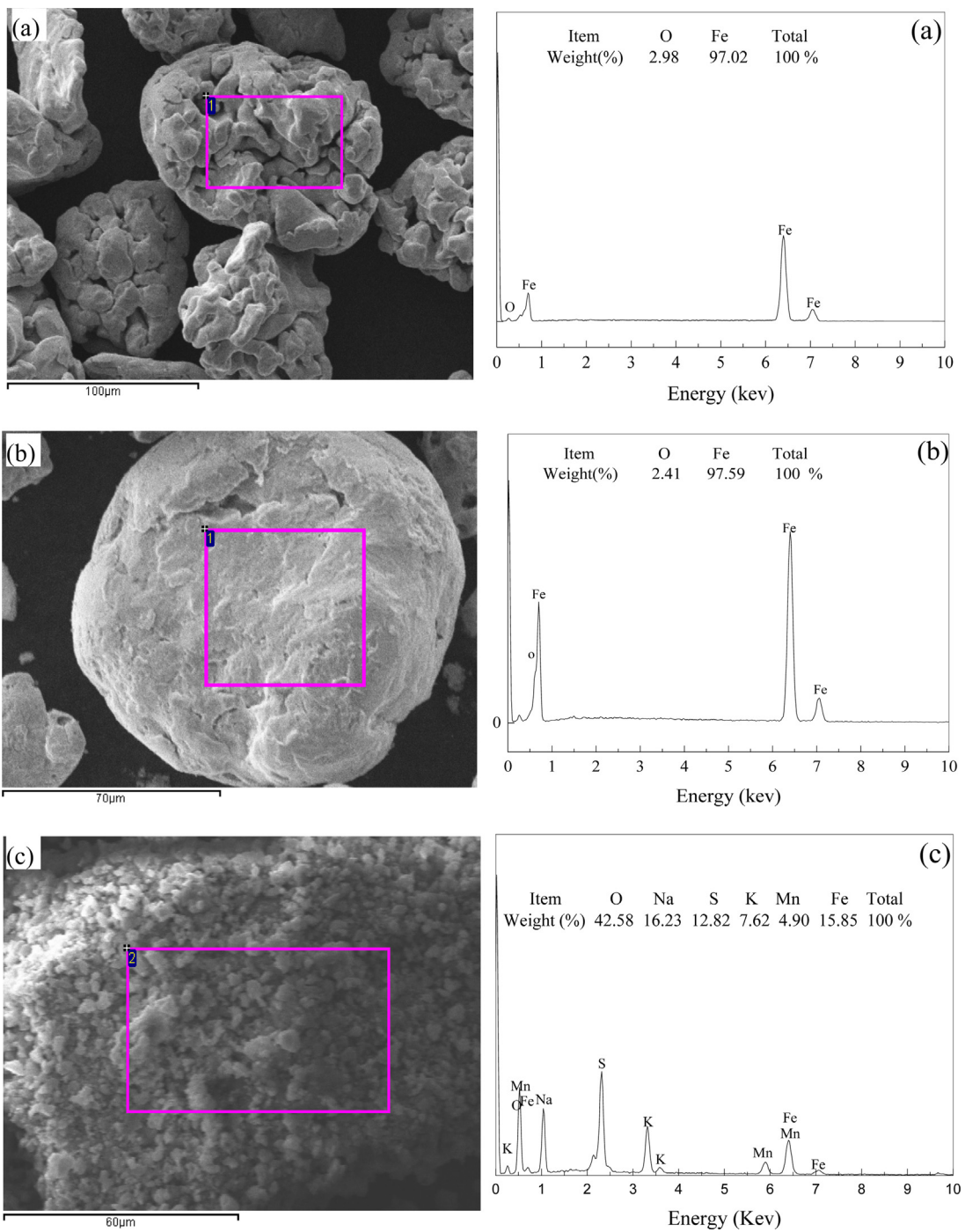


Fig. 8. SEM and EDS spectra of (a) reacted ZVI particles in Fe^0 system and (b) reacted ZVI particles and (c) generated flocculation in Fe^0 -PM-PS system.

maleic acid). Finally, most of them are degraded into CO_2 and H_2O . (ii) **direct oxidation:** PNP is oxidized directly to hydroquinone and *p*-benzoquinone, and then they are further transferred to fumaric acid and maleic acid. Finally, most of them were degraded completely. Therefore, a high COD removal (89.0%) was obtained after 120 min treatment by Fe^0 -PM-PS system.

3.6. Iron and manganese leaching during the processes

The pollutant degradation capacity of Fe^0 , Fe^0 -PM, Fe^0 -PS and Fe^0 -PM-PS systems was usually correlated with the corrosion of Fe^0 . After 120 min treatment, the total iron ions concentration (188.2 mg/L) in the effluent of Fe^0 -PM-PS system was higher than

those (6.4 mg/L, 6.1 mg/L and 108.2 mg/L) of Fe^0 , Fe^0 -PM and Fe^0 -PS control experiments (Fig. 7). The results suggest that the corrosion of Fe^0 could be improved remarkably by the combination PM and PS, which result in the higher reaction reactivity of Fe^0 -PM-PS system. The residual iron and manganese ions could be removed effectively through coagulating sedimentation under the alkaline condition (i.e., $\text{pH} = 7.0$ –9.0) [60], and its total manganese ions concentration could be decreased to 0.16 mg/L. According to the *Discharge standard of Pollutants for Municipal Wastewater Treatment Plant of China* (GB 18918–2002), the maximum permissible limit of Mn ions in effluent was 2.0 mg/L. Therefore, the residual Mn ions (0.16 mg/L) in the effluent cannot cause the secondary pollution.

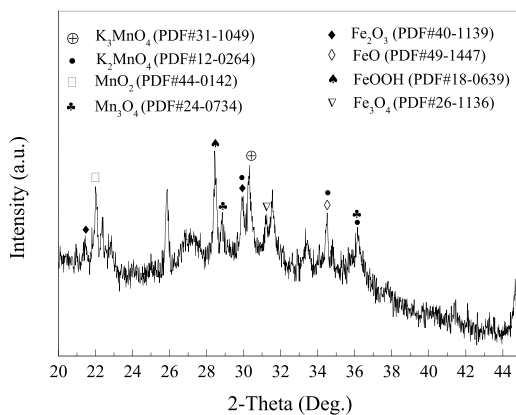


Fig. 9. XRD patterns of the generated flocculation in Fe^0 -PM-PS system after 120 min treatment.

3.7. Characteristics of the reacted Fe^0 particles and generated flocculation

Fig. 8 shows that the surface morphology and elemental composition of the reacted Fe^0 particles and generated flocculation in Fe^0 or Fe^0 -PM-PS process were observed by using SEM-EDS. **Fig. 8(a)** shows that only two elements of O (2.98 wt%) and Fe (97.02 wt%) were detected on the surface of the reacted Fe^0 particles in the Fe^0 process, and their morphology did not change seriously. The results could be explained that the higher initial pH (5.3) could not improve the corrosion of Fe^0 and obtained high treatment efficiency in the Fe^0 process [57]. The total iron ions concentration in the effluent of Fe^0 system was about 6.4 mg/L (**Fig. 7**). In particular, the extremely low COD removal (about 5.0%) was obtained after 120 min treatment by the Fe^0 process (**Fig. 3(c)**). After 120 min treatment by the Fe^0 -PM-PS process, however, the surface morphology of Fe^0 particles was changed from sponginess to smoothing (**Fig. 8(b)**). In addition, only a little oxygen (2.41 wt%) was detected on the surface of the reacted Fe^0 particles. The total iron ions concentration in the effluent of the Fe^0 -PM-PS process reached about 188.2 mg/L (**Fig. 7**). The results suggest that the Fe^0 particles were corroded seriously but only a little corrosion products were deposited on the Fe^0 surface in the Fe^0 -PM-PS process. In our previous work, however, it is clear that the corrosion products were easy to be deposited on the surface of Fe^0 particles and limit their reactivity seriously [61,62]. The results suggest that the oxidants (PS and PM) could improve the iron corrosion rate and provide the fresh Fe^0 particles from passivation. Guo and his colleagues also found that the typical oxidants (e.g., H_2O_2 , $KMnO_4$ and CrO_4^{2-}) can strongly activate the reactivity of ZVI through rapid corrosion of ZVI and continuous activation of passive layer [63].

Fig. 8(c) shows that O (42.58 wt%), Mn (4.90 wt%), Fe (15.85 wt%), S (12.82 wt%), K (7.62 wt%) and Na (16.23 wt%) were measured in the generated flocculation after 120 min treatment by the Fe^0 -PM-PS system. Meanwhile, only a little of Mn ions (0.16 mg/L) from the reduction of $KMnO_4$ was detected in the effluent of the Fe^0 -PM-PS system, which suggest that most of the metal ions were precipitated in the flocculation. The results indicate that $KMnO_4$ added in the Fe^0 -PM-PS system could not cause heavy metal pollution in the effluent.

3.8. XRD analysis of the generated flocculation in Fe^0 -PM-PS system

On the basis of SEM-EDS analysis, the generated flocculation in Fe^0 -PM-PS system was further analyzed by using XRD. **Fig. 9** shows that the crystallines including FeO , $FeOOH$, Fe_2O_3 , Fe_3O_4 , MnO_2 ,

Mn_3O_4 , K_2MnO_4 and K_2MnO_4 were detected by XRD. The iron oxides were from the corrosion of Fe^0 particles, while manganese oxides were from the reduction of PM. The generated oxides could be used to activate PS [64,65], which could remarkably improve the performance of the Fe^0 -PM-PS system.

3.9. XPS analysis of the generated flocculation in Fe^0 -PM-PS system

The chemical state of Fe, Mn, O and S of the generated flocculation in Fe^0 -PM-PS system was examined by XPS, and the results are shown in **Fig. 10**. The survey scan of the generated flocculation reveals the presence of Fe (2p), Mn (2p), O (1s), S (2p) and carbon whose C 1s peak (284.8 eV) was used to calibrate the acquired spectra, as seen in **Fig. 10(a)**. Further detailed scan have performed for Fe 2p, Mn 2p, O 1s and S 2p core level spectra to determine charge state of elements present in the flocculation. All XPS core level spectra were fitted using Shirley background.

The XPS survey scan of the Fe in the flocculation is shown in **Fig. 10(b)**. From this spectrum we can observe that $Fe\ 2p_{3/2}$ and $Fe\ 2p_{1/2}$ binding energy positions are 711.0 and 724.4 eV, which are very close to Fe^{3+} state in Fe_2O_3 at 710.7 and 724.3 eV, respectively [66,67]. Also, It has been reported that the peaks of $Fe\ 2p_{1/2}$ and $Fe\ 2p_{3/2}$ for iron oxides (i.e., hematite, maghemite and magnetite) are 723.2–724.8 eV and 710.6–711.2 eV, respectively [68]. The observed Fe 2p peak position corresponds to Fe^{3+} states, which suggest that the released Fe^{2+} ions from iron corrosion are easy to be oxidized in the presence of DO, PM and PS.

The profile of Mn 2p XPS spectra in the 632–662 eV range is showed in **Fig. 10(c)**. The binding energies at the 640.0–650.0 eV and 650.0–660.0 eV regions can be attributed to $Mn\ 2p_{3/2}$ and $Mn\ 2p_{1/2}$, respectively [69]. **Fig. 10(c)** shows five main peaks belongs to Mn(II) ($Mn\ 2p_{3/2}$: 641.2 eV and 647.0 eV), Mn(IV) ($Mn\ 2p_{3/2}$: 642.6 eV), Mn(VI) ($Mn\ 2p_{3/2}$: 644.2 eV) [70] and $Mn\ 2p_{1/2}$ for Mn(III) at 653.1 eV, respectively.

The high-resolution scan of the O 1s core level is depicted in **Fig. 10(d)**. The spectrum shows the presence of two peaks at 531.4 eV and 529.7 eV. According to literatures, the peak at 529.7–530.1 eV corresponds to O^{2-} , and the peak at 531.1–531.7 eV can be attributed to surface-adsorbed oxygen species (i.e., O_2^{2-} , O^- , OH^-) [69]. The reason is primarily attributed to the formation of manganite or iron (hydro)oxides. **Fig. 10(e)** describes S 2p XPS spectra from 160.0 to 176.0 eV, and the doublet located at 168.2 and 169.4 eV are due to the reaction produce of SO_4^{2-} [71].

3.10. Reaction mechanism of the Fe^0 -PM-PS process

According to the analysis results of EDS, XRD and XPS, it could be concluded that Fe^{2+} , Fe^{3+} , Mn^{n+} , FeO , $FeOOH$, Fe_2O_3 , Fe_3O_4 , MnO_2 , Mn_2O_3 , Mn_3O_4 , K_2MnO_4 , K_2MnO_4 were detected in the Fe^0 -PM-PS process. Furthermore, most of these products could be used to activate PS and enhance the treatment efficiency of the Fe^0 -PM-PS process. There would be a strong synergistic effect in the Fe^0 -PM-PS system, and their reaction mechanisms were illustrated thoroughly in the following (see **Fig. 11**):

3.10.1. Synergistic effect between Fe^0 and PS

The addition of PS would decrease seriously the pH of reaction solution (Eqs. (19)–(20)) [51,72]. Under the acidic condition, Fe^0 could be corroded rapidly and release a plenty electrons and Fe^{2+} . Meanwhile, H^+ ions could accept the electrons and generate free hydrogen ([H]) that could rapidly deoxygenate the pollutants [73,74]. For example, a plenty PNP was directly deoxygenated to *p*-aminophenol (223 mg/L) in the initial 30 min treatment in the Fe^0 -PM-PS process (see **Fig. 5(a)**). In addition, the Fenton-like reaction would be formed in the presence of dissolved oxygen (DO)

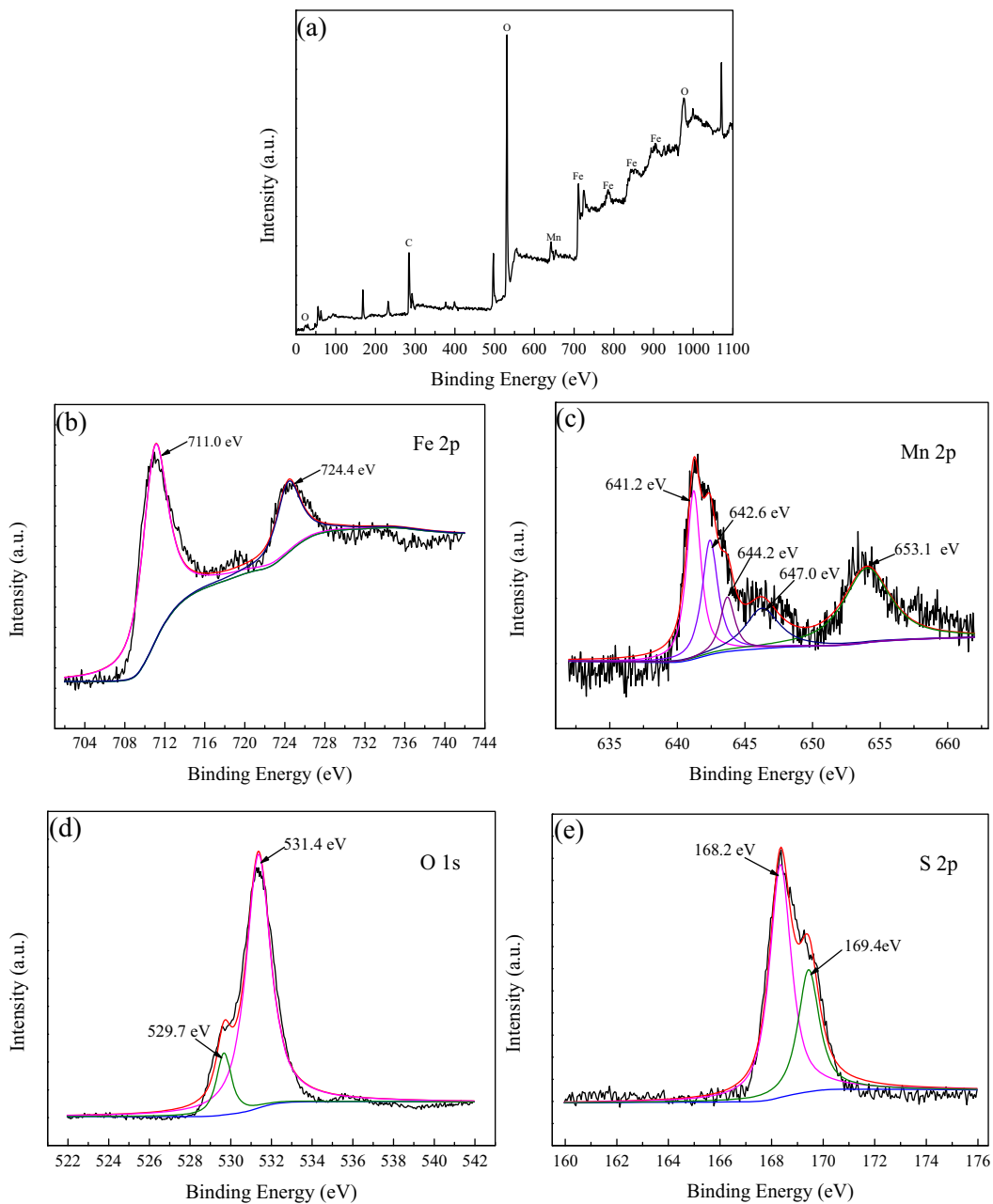


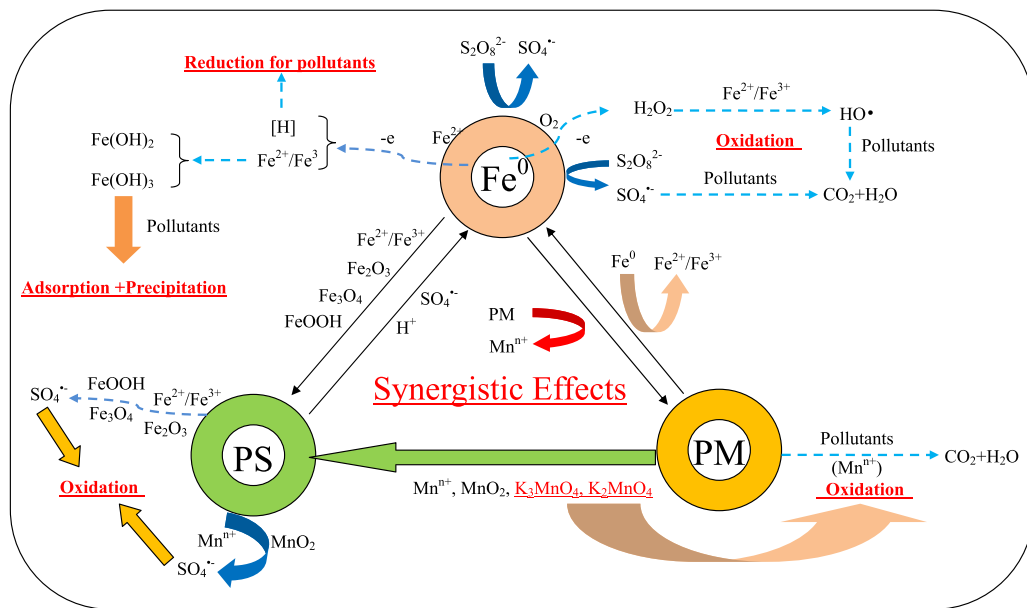
Fig. 10. XPS spectra of the generated flocculation in the Fe^0 -PM-PS system, (a) full-range scan of the samples, (b) Fe 2p core level, (c) Mn 2p core level, (d) O 1s core level and (e) S 2p core level.

[7]. However, Fig. 1(f) shows that the performance of the Fe^0 -PM-PS system was not affected by the change of aeration because the Fenton-like reaction could be neglected when the enough other oxidants (i.e., PS and PM) were added. Furthermore, the oxidants can strongly activate the reactivity of Fe^0 through rapid corrosion of Fe^0 and continuous activation of passive layer [63]. For example, only a little of oxides could be found on the surface of the reacted Fe^0 in the Fe^0 -PM-PS system (see Fig. 8(b)).

The corrosion products of Fe^0 including Fe^{2+} , Fe^{3+} , FeO , FeOOH , Fe_2O_3 , Fe_3O_4 could be used to activate the PS effectively in the Fe^0 -PM-PS system. In a word, PS could accelerate the corrosion rate of Fe^0 and generate a plenty of corrosion products, which would accelerate the activation of PS in return [33,51].

3.10.2. Synergistic effect between Fe^0 and PM

PM can also strongly activate the reactivity of Fe^0 through rapid corrosion of Fe^0 and continuous activation of passive layer [63], which facilitate the formation of [H] or Fenton-like reaction in Fe^0 process. Furthermore, the generated manganese (hydr) oxides, iron hydroxides and Mn-Fe oxide could improve the degradation of the PNP by oxidation and adsorption [63]. Meanwhile, a similar results were reported that methylene blue (MB) could be removed effectively by the synergistic technology based on nano zero-valent iron (NZVI) and potassium permanganate (PM) [49]. In addition, the pollutants could be oxidized directly by PM and its products (e.g., K_3MnO_4 , K_2MnO_4).

Fig. 11. Reaction mechanism of the Fe^0 -PM-PS process.

3.10.3. Synergistic effect between PM and PS

The reduction products of PM including Mn^{n+} , MnO_2 , Mn_2O_3 , Mn_3O_4 , K_3MnO_4 , K_2MnO_4 can be used to activate PS, which can improve the performance of the Fe^0 -PM-PS system [46,64,75]. Sun and his colleagues have found that bisulfite could activate manganese oxidants and enhance their oxidation capacity for the organic contaminants [32]. Thus, PM might also be activated effectively by PS, which could improve the performance of the Fe^0 -PM-PS system. However, COD removal (16.3%) obtained by PM-PS was much lower than that (32.2%) of PM alone (see Fig. 4(b)). The results suggest that the oxidation capacity of PM can be limited directly by PS. But their synergistic effect will be occurred when the Fe^0 was added in the treatment system.

4. Conclusions

A Fe^0 -PM-PS system was developed to decompose the PNP in aqueous solution. First, single-factor experiment and response surface methodology (RSM) were used to optimize the main experimental parameters, and the optimal conditions (i.e., Fe^0 dosage of 11.9 g/L, PM of 15.0 mmol/L, PS of 18.1 mmol/L and feeding times of oxidants of 4) was obtained. COD removal efficiency (i.e., 89.0% after 120 min treatment) obtained by the Fe^0 -PM-PS process was much higher than those of Fe^0 , PM, PS, Fe^0 -PM, Fe^0 -PS and PM-PS systems (i.e., 5.0%, 32.2%, 1.7%, 27.7%, 23.1%, and 16.3% after 120 min treatment, respectively), which confirm the superiority of the Fe^0 -PM-PS process. Besides, the contradistinctive analysis of UV-vis spectra of the effluent in seven systems further confirms the synergistic effect of the Fe^0 -PM-PS process. Furthermore, the results of total iron concentration in Fe^0 , Fe^0 -PM, Fe^0 -PS and Fe^0 -PM-PS systems demonstrate that the addition of PM and PS could improve the corrosion rate of Fe^0 rapidly. In addition, the intermediates were measured by HPLC, and the PNP degradation pathway was proposed. The results suggest that PNP was decomposed by the combined reduction and oxidation. According to the analysis results of EDS, XRD and XPS, it could be concluded that Fe^{2+} , Fe^{3+} , Mn^{n+} , FeO , FeOOH , Fe_2O_3 , Fe_3O_4 , MnO_2 , Mn_2O_3 , Mn_3O_4 , K_3MnO_4 , K_2MnO_4 were detected in the Fe^0 -PM-PS process. All the results indicate that there would be a strong synergistic effect in the Fe^0 -PM-PS system, which play a leading role in the degradation of the

pollutants. Therefore, the Fe^0 -PM-PS process would be a promising technology for the toxic and refractory industrial wastewater.

Acknowledgments

The authors would like to acknowledge the financial support from National Natural Science Foundation of China (No. 21207094), and Fundamental Research Funds for the Central Universities (No. 2015SCU04A09).

References

- [1] B. Lai, Y.H. Zhang, Z.Y. Chen, P. Yang, Y.X. Zhou, J.L. Wang, *Appl. Catal. B: Environ.* 144 (2014) 816–830.
- [2] B. Lai, Y.H. Zhang, R. Li, Y.X. Zhou, J.L. Wang, *Chem. Eng. J.* 249 (2014) 143–152.
- [3] F. Fu, D.D. Dionysiou, H. Liu, *J. Hazard. Mater.* 267 (2014) 194–205.
- [4] A. Ghauch, *Freib. Online Geol.* 38 (2015) 1–80.
- [5] X. Guan, Y. Sun, H. Qin, J. Li, I.M.C. Lo, D. He, H. Dong, *Water Res.* 75 (2015) 224–248.
- [6] B. Lai, Z.Y. Chen, Y.X. Zhou, P. Yang, J.L. Wang, Z.Q. Chen, *J. Hazard. Mater.* 250–251 (2013) 220–228.
- [7] K.S. Wang, C.L. Lin, M.C. Wei, H.H. Liang, H.C. Li, C.H. Chang, Y.T. Fang, S.H. Chang, *J. Hazard. Mater.* 182 (2010) 886–895.
- [8] C. Martínez, M. Canle L, M.I. Fernández, J.A. Santaballa, J. Faria, *Appl. Catal. B: Environ.* 102 (2011) 563–571.
- [9] T.E. Doll, F.H. Frimmel, *Water Res.* 39 (2005) 403–411.
- [10] F. Qi, W. Chu, B. Xu, *Chem. Eng. J.* 262 (2015) 552–562.
- [11] H. Li, B. Xu, F. Qi, D. Sun, Z. Chen, *Appl. Catal. B: Environ.* 152 (2014) 342–351.
- [12] A. Ghauch, H. Baydoun, P. Dermesopian, *Chem. Eng. J.* 172 (2011) 18–27.
- [13] C.M. Dai, X.F. Zhou, Y.L. Zhang, Y.P. Duan, Z.M. Qiang, T.C. Zhang, *Environ. Technol.* 33 (2012) 1101–1109.
- [14] M.G. Antoniou, A.A. de la Cruz, D.D. Dionysiou, *Appl. Catal. B: Environ.* 96 (2010) 290–298.
- [15] Y.-T. Lin, C. Liang, J.-H. Chen, *Chemosphere* 82 (2011) 1168–1172.
- [16] S. Yang, P. Wang, X. Yang, G. Wei, W. Zhang, L. Shan, *J. Environ. Sci.* 21 (2009) 1175–1180.
- [17] K.-C. Huang, R.A. Couttenye, G.E. Hoag, *Chemosphere* 49 (2002) 413–420.
- [18] J. Criquet, N. Karpel Vel Leitner, *Chem. Eng. J.* 169 (2011) 258–262.
- [19] S.O.B. Boukari, F. Pellizzari, N. Karpel Vel Leitner, *J. Hazard. Mater.* 185 (2011) 844–851.
- [20] P. Gayathri, R. Praveena Juliya Dorathi, K. Palanivelu, *Ultrason. Sonochem.* 17 (2010) 566–571.
- [21] O.S. Furman, A.L. Teel, M. Ahmad, M.C. Merker, R.J. Watts, *J. Environ. Eng.* 137 (2011) 241–247.
- [22] A. Rastogi, S.R. Al-Abed, D.D. Dionysiou, *Appl. Catal. B: Environ.* 85 (2009) 171–179.
- [23] S.-Y. Oh, H.-W. Kim, J.-M. Park, H.-S. Park, C. Yoon, *J. Hazard. Mater.* 168 (2009) 346–351.
- [24] A. Ghauch, G. Ayoub, S. Naim, *Chem. Eng. J.* 228 (2013) 1168–1181.

[25] X. Xiong, B. Sun, J. Zhang, N. Gao, J. Shen, J. Li, X. Guan, *Water Res.* 62 (2014) 53–62.

[26] S.-Y. Oh, S.-G. Kang, P.C. Chiu, *Sci. Total Environ.* 408 (2010) 3464–3468.

[27] A. Tsitonaki, B. Petri, M. Crimi, H. Mosbæk, R.L. Siegrist, P.L. Bjerg, *Crit. Rev. Environ. Sci. Technol.* 40 (2010) 55–91.

[28] S.Y. Oh, S.G. Kang, P.C. Chiu, *Sci. Total Environ.* 408 (2010) 3464–3468.

[29] B. Sun, X. Guan, J. Fang, P.G. Tratnyek, *Environ. Sci. Technol.* 49 (2015) 12414–12421.

[30] K.A.M. Ahmed, J. Taibah Univ. Sci. 10 (2016) 412–429.

[31] L. Li, D. Wei, G. Wei, Y. Du, *Chemosphere* 149 (2016) 279–285.

[32] B. Sun, X. Guan, J. Fang, P.G. Tratnyek, *Environ. Sci. Technol.* 49 (2015) 12414–12421.

[33] W.-D. Oh, Z. Dong, T.-T. Lim, *Appl. Catal. B: Environ.* 194 (2016) 169–201.

[34] E. Ghafari, H. Costa, E. Júlio, *Constr. Build. Mater.* 66 (2014) 375–383.

[35] K. Anupam, S. Dutta, C. Bhattacharjee, S. Datta, *Can. J. Chem. Eng.* 89 (2011) 1274–1280.

[36] J.M. Monteagudo, A. Durán, R. González, A.J. Expósito, *Appl. Catal. B: Environ.* 176–177 (2015) 120–129.

[37] S. Madadi, M. Sohrabi, S.J. Royaee, *J. Taiwan Inst. Chem. Eng.* 55 (2015) 101–111.

[38] K. Anupam, S. Dutta, C. Bhattacharjee, S. Datta, *Chem. Eng. J.* 173 (2011) 135–143.

[39] K. Anupam, A.K. Sharma, P.S. Lal, S. Dutta, S. Maity, *Energy* 106 (2016) 743–756.

[40] L.W. Matzek, K.E. Carter, *Chemosphere* 151 (2016) 178–188.

[41] C. Liang, I.L. Lee, I.Y. Hsu, C.-P. Liang, Y.-L. Lin, *Chemosphere* 70 (2008) 426–435.

[42] G.V. Buxton, T.N. Malone, G.A. Salmon, *J. Chem. Soc. Faraday Trans.* 93 (1997) 2893–2897.

[43] J.L. Wang, L.J. Xu, *Crit. Rev. Environ. Sci. Technol.* 42 (2012) 251–325.

[44] S. Gao, J. Cui, Y. Xiong, W. Xiao, D. Wang, A.N. Alshawabkeh, X. Mao, *Sep. Purif. Technol.* 144 (2015) 248–255.

[45] E. Saputra, S. Muhammad, H. Sun, H.M. Ang, M.O. Tadé, S. Wang, *Environ. Sci. Technol.* 47 (2013) 5882–5887.

[46] E. Saputra, S. Muhammad, H. Sun, H.-M. Ang, M.O. Tadé, S. Wang, *Appl. Catal. B: Environ.* 154–155 (2014) 246–251.

[47] S. Li, G. Zhang, P. Wang, H. Zheng, Y. Zheng, *Chem. Eng. J.* 294 (2016) 371–379.

[48] Y. Li, J. Sun, S.-P. Sun, J. Hazard. Mater. 313 (2016) 193–200.

[49] X. Wang, P. Liu, M. Fu, J. Ma, P. Ning, *Chemosphere* 155 (2016) 39–47.

[50] M. Nie, C. Yan, M. Li, X. Wang, W. Bi, W. Dong, *Chem. Eng. J.* 279 (2015) 507–515.

[51] X. Zou, T. Zhou, J. Mao, X. Wu, *Chem. Eng. J.* 257 (2014) 36–44.

[52] H. Kusic, I. Peternel, S. Ukić, N. Koprivanac, T. Bolanca, S. Papic, A.L. Božić, *Chem. Eng. J.* 172 (2011) 109–121.

[53] C. Liang, Z.-S. Wang, C.J. Bruell, *Chemosphere* 66 (2007) 106–113.

[54] Y. Segura, F. Martínez, J.A. Melero, *Appl. Catal. B: Environ.* 136–137 (2013) 64–69.

[55] K. Anupam, V. Swaroop, Deepika, P.S. Lal, V. Bist, *Ecol. Eng.* 82 (2015) 26–39.

[56] P. Gupta, P. Parkhey, *Bioresour. Technol.* 173 (2014) 207–215.

[57] B. Lai, Y.X. Zhou, H.K. Qin, C.Y. Wu, C.C. Pang, Y. Lian, J.X. Xu, *Chem. Eng. J.* 179 (2012) 1–7.

[58] M. Martín-Hernández, J. Carrera, M.E. Suárez-Ojeda, M. Besson, C. Descorme, *Appl. Catal. B: Environ.* 123–124 (2012) 141–150.

[59] M. Martín-Hernández, J. Carrera, M.E. Suárez-Ojeda, M. Besson, C. Descorme, *Appl. Catal. B: Environ.* 123–124 (2012) 141–150.

[60] D.S. Patil, S.M. Chavan, J.U.K. Oubagaranadin, *J. Environ. Chem. Eng.* 4 (2016) 468–487.

[61] C. Liang, C.-F. Huang, N. Mohanty, R.M. Kurakalva, *Chemosphere* 73 (2008) 1540–1543.

[62] B. Lai, Y.X. Zhou, P. Yang, *Ind. Eng. Chem. Res.* 51 (2012) 7777–7785.

[63] X. Guo, Z. Yang, H. Liu, X. Lv, Q. Tu, Q. Ren, X. Xia, C. Jing, *Sep. Purif. Technol.* 146 (2015) 227–234.

[64] H. Liang, H. Sun, A. Patel, P. Shukla, Z.H. Zhu, S. Wang, *Appl. Catal. B: Environ.* 127 (2012) 330–335.

[65] Y. Leng, W. Guo, X. Shi, Y. Li, A. Wang, F. Hao, L. Xing, *Chem. Eng. J.* 240 (2014) 338–343.

[66] A. Mašić, A.T.L. Santos, B. Etter, K.M. Udert, K. Villez, *Water Res.* 85 (2015) 244–254.

[67] A.J. Chen, X.M. Wu, Z.D. Sha, L.J. Zhuge, Y.D. Meng, *J. Phys. D: Appl. Phys.* 39 (2006) 4762.

[68] S.-H. Do, Y.-J. Kwon, S.-J. Bang, S.-H. Kong, *Chem. Eng. J.* 221 (2013) 72–80.

[69] M. Piumetti, D. Fino, N. Russo, *Appl. Catal. B: Environ.* 163 (2015) 277–287.

[70] W. Fredriksson, K. Edström, C.O.A. Olsson, *Corros. Sci.* 52 (2010) 2505–2510.

[71] M.D. Croitoru, *J. Chromatogr. B* 911 (2012) 154–161.

[72] G. Ayoub, A. Ghauch, *Chem. Eng. J.* 256 (2014) 280–292.

[73] B. Lai, Y.X. Zhou, P. Yang, J.H. Yang, J.L. Wang, *Chemosphere* 90 (2013) 1470–1477.

[74] H. Cheng, W. Xu, J. Liu, H. Wang, Y. He, G. Chen, *J. Hazard. Mater.* 146 (2007) 385–392.

[75] Y. Wang, H. Sun, H.M. Ang, M.O. Tadé, S. Wang, *Appl. Catal. B: Environ.* 164 (2015) 159–167.